Impulse studies of double diffraction: A discrete Huygens interpretation

Herman Medwin, Emily Childs,[a] and Gary M. Jebsen[b]
Physics Department, Naval Postgraduate School, Monterey, California 93940

(Received 21 March 1982; accepted for publication 8 May 1982)

A closed-form analytical impulse solution of diffraction by a rigid wedge is interpreted from the point of view of discrete Huygens wavelets emanating from the crest of the wedge. The strengths of these secondary sources and the impulse field diffracted over a second wedge are calculated. Digital Fourier transformation is then used to determine the spectral loss during double diffraction. The technique is applied to a thick plate, an angled wide barrier, and a strip; successful predictions of laboratory experiments are achieved. In principle, the method may be used for any number of diffractions by straight line segments of an extended barrier or scattering surface.

PACS numbers: 43.20.Bi, 43.20.Fn, 43.30.Gv, 43.30.Ft

INTRODUCTION

Time domain (impulse) descriptions of diffraction and reflection can provide a unique picture of the contributions of Huygens impulse wavelets in a complex scattering problem. For this and other reasons, most experimental studies of scattering use impulse sources. However, although the theoretical literature of diffraction and reflection by wedges and plates is endowed with a wealth of solutions for continuous wave (cw) sources[1] there have been very few impulse solutions of these same fundamental problems.[2,3] Very recently, an analytical transform of the classical cw solution for diffraction by wedges has been accomplished.[4]

Previously we have shown[5] how the normal coordinate solution of reflection and diffraction of a delta function impulse by an infinite rigid wedge can be adapted to provide computer-assisted calculations of the impulse and spectral scattering for a *finite* wedge. This adaptation completely avoids the flaws of the Kirchhoff assumption, which is now known[6–8] to lead to order-of-magnitude errors at near grazing incidence. The technique appears to have application to a wide range of problems such as designing noise barriers and predicting scatter from a rough surface.

At this time a discrete Huygens impulse interpretation of double diffraction is considered. Scatter from one edge and rescatter from a nearby edge can produce acoustic pressures that are significantly different from the separate diffractions. Again the impulse technique distinguishes the diffraction contributions from different parts of the edges and clarifies the importance of each, and again finite edges can be handled without the Kirchhoff assumption. Furthermore in our technique the two diffracting edges need not be parallel; closeness to the barrier is not an impediment to the solution; ranges and barrier thickness can have any value. Validation of this discrete Huygens interpretation is accomplished here by comparison with a cw analytical solution[4] and results of experiments performed in our anechoic laboratory.[6,9]

Double diffraction plays an important part in scatter from a slit, strip, thick noise barrier, and probably at near grazing multiple scatter from a rough surface. The technique described here appears to possess advantages over other schemes that have been employed; it is simple, it avoids the Kirchhoff assumption, it is a clear and direct digital application of the conceptually appealing Huygens' principle.

I. SINGLE WEDGE DISCRETE HUYGENS WAVELETS

When an impulse from a delta function point source diffracts over a wedge, the spherically diverging wave creates, first, a delta function via the least time path, then weaker contributions as the wave scatters from either side of the least time intercept. It thereby appears as a phased continuous line source which radiates energy from the edge.

The Biot and Tolstoy boundary diffraction wave[3] takes a particularly simple form when their doublet source is replaced by a delta function acceleration source.[5] The expression is given in Eqs. (1)–(3) for the geometry shown in Fig. 1. The distance coordinates are more easily visualized and calculated in the unfolded geometry of Fig. 1(b).

$$p(t) = (-S\rho c/4\pi\theta_w)\{\beta\}(rr_0 \sinh Y)^{-1}\exp(-\pi Y/\theta_w), \quad (1)$$

where

$$\beta = \sin[(\pi/\theta_w)(\pi \pm \theta \pm \theta_0)] \times \{1 - 2\exp(-\pi Y/\theta_w)\cos[(\pi/\theta_w)(\pi \pm \theta \pm \theta_0)] + \exp(-2\pi Y/\theta_w)\}^{-1}, \quad (2)$$

$$Y = \operatorname{arc\,cosh} \frac{c^2t^2 - (r^2 + r_0^2 + Z^2)}{2rr_0}. \quad (3)$$

The term $(\pi + \theta \pm \theta_0)$ is written for simplicity; the curly bracket consists of the sum of four terms obtained by using the four possible combinations of the angles, $\pm\theta$ and $\pm\theta_0$.

Source coordinates are $(r_0,\theta_0,0)$; receiver coordinates are (r,θ,Z). The angle of the wedge measured in the fluid region is called θ_w, see Fig. 1(a). Note that the thin plate or semi-infinite screen is a wedge with $\theta_w = 2\pi$.

The least time over the wedge is

$$\tau_0 = [(r + r_0)^2 + Z^2]^{1/2}/c. \quad (4)$$

It is convenient to express the total time t in terms of the least time τ_0 plus the later incremental time τ

[a] Ocean Acoustics Associates.
[b] Permanent address: David Taylor NSRDC, Bethesda, MD 20084.

 © 1982 Acoustical Society of America

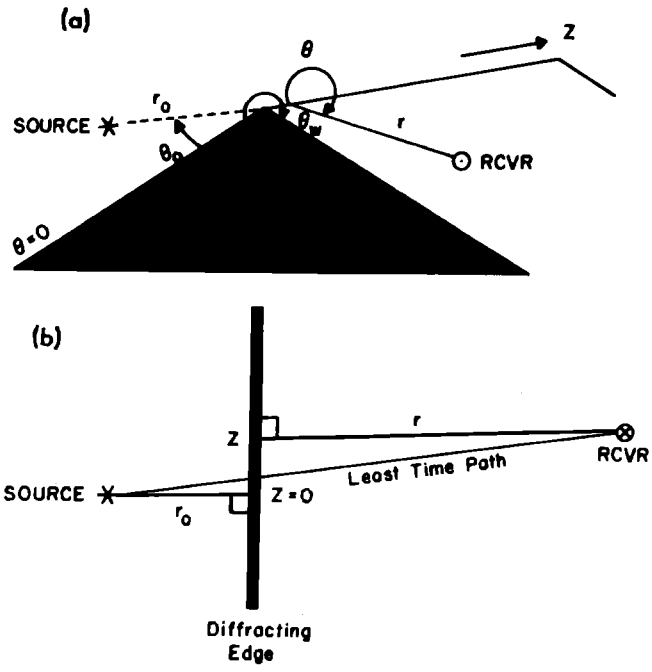

FIG. 1. (a) Wedge geometry for Eqs. (1)–(3); (b) unfolded geometry.

$$t = \tau_0 + \tau. \tag{5}$$

Then

$$Y = \operatorname{arc\,cosh}\left(\frac{c^2(2\tau_0\tau + \tau^2)}{2rr_0} + 1\right) \tag{6}$$

and

$$(\sinh Y)^{-1} = \left[\left(\frac{c^2\tau_0\tau}{rr_0} + \frac{c^2\tau^2}{2rr_0} + 1\right)^2 - 1\right]^{-1/2}. \tag{7}$$

The largest diffraction contributions occur for incremental times small compared to the least time; there, useful approximations are

$$\lim_{\tau \ll \tau_0} (rr_0 \sinh Y)^{-1} \to (2\tau_0\tau c^2 r_0 r)^{-1/2} \tag{8}$$

$$\lim_{\tau \ll \tau_0} \exp(-\pi Y/\theta_w) \to 1 - \frac{\pi}{\theta_w} M + \frac{\pi}{\theta_w}\left(\frac{\pi}{\theta_w} + 1\right)\frac{M^2}{2} + \cdots, \tag{9}$$

where $M = A + A^2/2 + A^3/8 + \cdots$ and $A = [c\tau_0/(rr_0)^{1/2}] \times (2\tau/\tau_0)^{1/2}$. Use

$$Y = \operatorname{arc\,cosh} x = \ln[x + (x^2 - 1)^{1/2}].$$

Then, provided that θ is not close to the geometrical shadow boundary, when $\tau/\tau_0 \ll 1$, β of Eq. (2) approaches a constant. Then (1), (8), and (9) lead to the instantaneous pressures at the receiver $p(\tau) = B\tau^{-1/2}$ for $\tau \ll \tau_0$, where

$$B = S\rho\beta/[4\pi\sqrt{2}\theta_w(\tau_0 rr_0)^{1/2}] \tag{10}$$

and the diffracted spectral pressure, obtained by the Fourier transformation, has the frequency dependence

$$P_D(f) \sim f^{-1/2}. \tag{11}$$

The relation is a useful guide to acoustical engineers in the design of noise barriers.

The preceding neat analysis breaks down when the diffracted sound direction is near the geometrical shadow boundary or near the reflection direction. To see this, near the shadow boundary write

$$\theta = \theta_0 + \pi + \epsilon, \tag{12}$$

where ϵ = angle into the shadow measured from the geometrical shadow boundary. The interesting terms of β in (2) depend on

$$\phi = (\pi/\theta_w)(\pi \pm \theta \pm \theta_0).$$

For example, using ϕ with subscripts to indicate the sequence of signs in ϕ, near the shadow boundary we have

$$\begin{aligned} \phi_{++} &= (2\pi/\theta_w)(\pi + \theta_0 + \epsilon/2), \\ \phi_{+-} &= (2\pi/\theta_w)(\pi + \epsilon/2), \\ \phi_{-+} &= (2\pi/\theta_w)(-\epsilon/2), \\ \phi_{--} &= (2\pi/\theta_w)(-\theta_0 - \epsilon/2). \end{aligned} \tag{13}$$

The $-+$ term of the β bracket is easy to analyze because it does not depend on θ_0,

$$\beta_{-+} = \sin\left[\left(\frac{2\pi}{\theta_w}\right)\left(-\frac{\epsilon}{2}\right)\right] \times \left\{1 - 2\left(1 - \frac{\pi}{\theta_w}M + \cdots\right)\cos\left[\left(\frac{2\pi}{\theta_w}\right)\left(-\frac{\epsilon}{2}\right)\right] + \left(1 - \frac{2\pi}{\theta_w}M + \cdots\right)\right\}^{-1}. \tag{14}$$

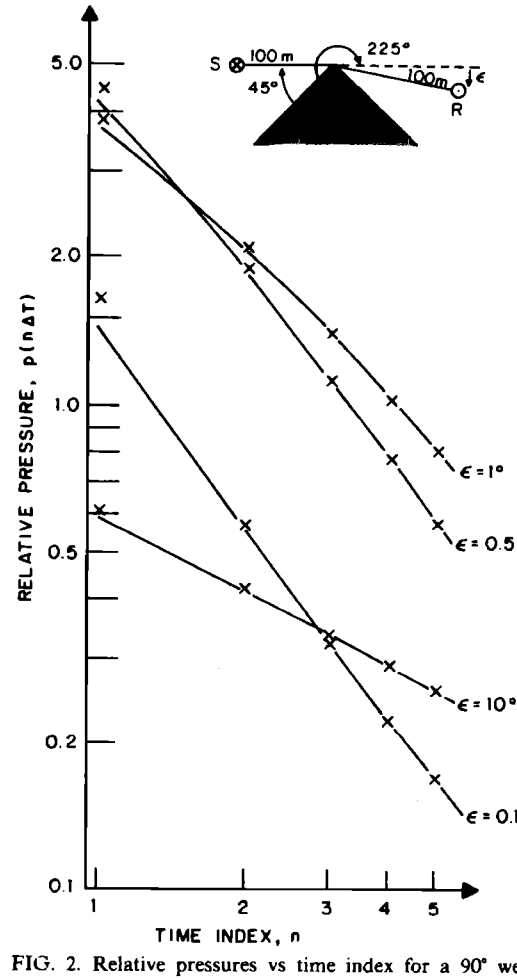

FIG. 2. Relative pressures vs time index for a 90° wedge, $\theta_w = 270°$, $\theta_0 = 45°$, $\theta = 225° + \epsilon$, $r = 100$ m, $r_0 = 100$ m. The four values of ϵ are angles of penetration into geometrical shadow region: The solid lines are instantaneous values from Eq. (1). Crosses are average values calculated from Eq. (17).

Considering the direction close to the shadow boundary, $\epsilon \ll \pi/2$, we look at the simple case of diffraction by a plate, $\theta_w = 2\pi$, and expand the trigonometric functions of small angle ($\phi_{-+} = -\epsilon/2$):

$$\beta_{-+} \simeq \frac{-\epsilon/2}{1 - 2(1 - M/2 + \frac{1}{8}M^2 \cdots)(1 - \epsilon^2/8) + (1 - M + M^2 \cdots)} \simeq \frac{-\epsilon/8}{M^2 + \epsilon^2}, \quad \text{for } \Delta T/\tau_0 \ll 1, \quad \epsilon \ll \pi/2, \quad \theta_w = 2\pi. \tag{15}$$

In (15), which is in many ways typical of the β terms, it is clearly seen that the assumption which led to (10) holds only when

$$\epsilon \gg M \simeq A$$

or, approximately,

$$\epsilon \gg [c\tau_0/(rr_0)^{1/2}](\tau/\tau_0)^{1/2}. \tag{16}$$

Digitally, the pressure is presented at temporal separations ΔT, and the incremental time after the least time is $\tau = n\Delta T$, where n = integer. The digital time lags $n\Delta T$ are the "milestones" of the temporal response.

Results of a more complete numerical analysis for one case are shown in Fig. 2 where it is seen that, for a delta function source, as the geometrical shadow boundary is approached, smaller ϵ, the impulse changes from a $(\tau)^{-1/2}$ dependence as in (10) to a much steeper slope. The frequency spectrum, Fig. 3, moves from $f^{-1/2}$, at larger ϵ, as in (11), to a nearly flat spectrum f^0 (at $\epsilon = 0.1°$) which would correspond to a delta function in time.

In Figs. 1(b) and 4 the delta function pulse is received first at time τ_0, having traveled the least time path from source to receiver. Later dual arrivals come from points on both sides of the least time crossing of the edge. The later crossing points are positions on ellipses with focal points at source and receiver.

The pressures at the receiver are converted to discrete values at intervals $n\Delta T$ by defining the mean value of width ΔT centered on $n\Delta T$

$$\langle p(n\Delta T)\rangle = \frac{1}{\Delta T}\int_{(n-1/2)\Delta T}^{(n+1/2)\Delta T} p(t)\,dt, \tag{17}$$

where $p(t)$ is given by Eq. (1). Under the conditions of (10) the discrete pressures at $n\Delta T$ are given by

$$\langle p(\tau)\rangle_{n>1} = \frac{B}{\Delta T}\int_{(n-1/2)\Delta T}^{(n+1/2)\Delta T} \tau^{-1/2}d\tau = B(2/\Delta T)^{1/2}[(2n+1)^{1/2} - (2n-1)^{1/2}]. \tag{18}$$

A finite value is obtained for the least time interval $0\Delta T$ by performing the integration with zero pressure for $-\Delta T/2 \leqslant \tau \leqslant 0$ and is

$$\langle(p(\tau)\rangle_{n=0} = \beta(2/\Delta T)^{1/2}. \tag{19}$$

It is interesting to observe from (18) and (19) that, provided the received signal direction is not close to the shadow

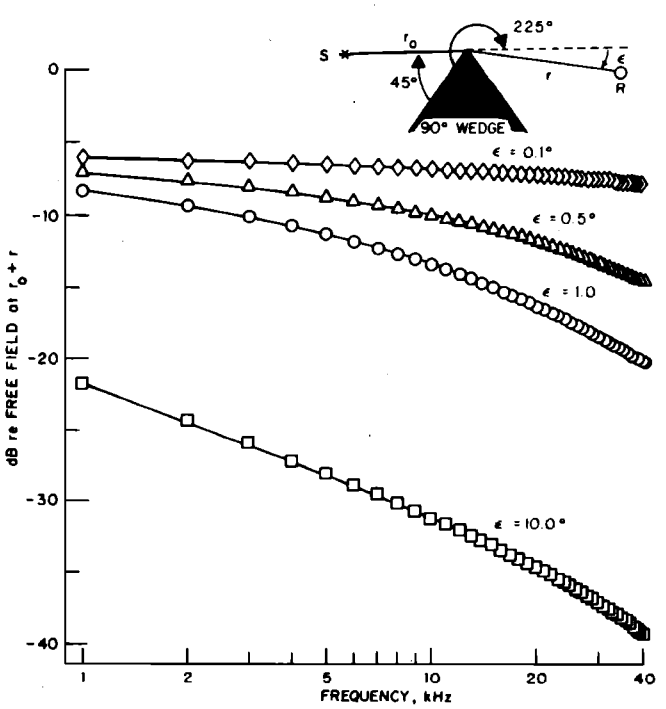

FIG. 3. Spectra of diffracted energy as a function of angle of penetration into geometrical shadow region. Curves are the Fourier transforms of those in Fig. 2.

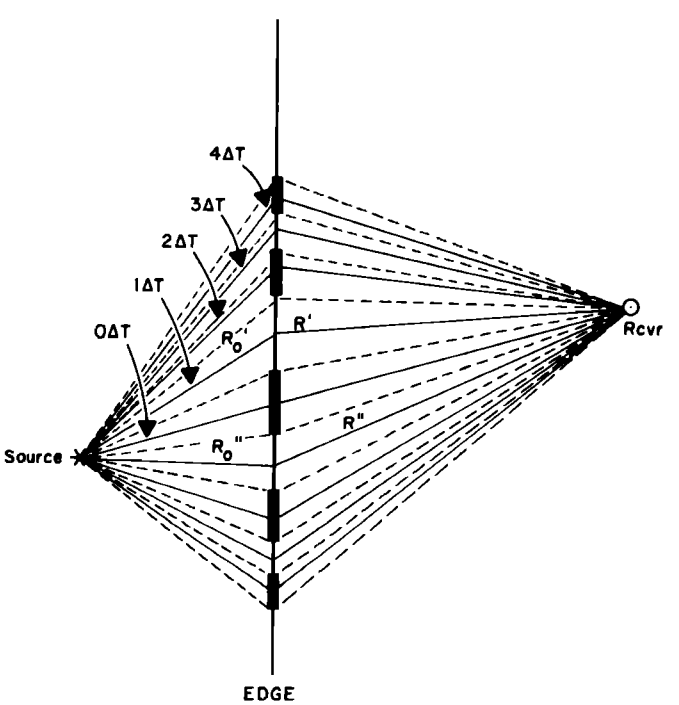

FIG. 4. Unfolded geometry showing discrete paths (solid lines) and their $\pm\frac{1}{2}\Delta T$ boundaries (dashed lines) from source to receiver. Discrete time lags are relative to least time path. Diffracting edge segments for even-ordered time lags $0\Delta T$, $\pm 2\Delta T$, $\pm 4\Delta T$, have been shaded for clarity. The ranges $R_0' + R'$ and $R_0'' + R''$ as defined and used in Eqs. (27)–(30) are shown for the two paths at $1\Delta T$ lag.

boundary or the reflection direction, these discrete values bear a constant relation to one another independent of geometry and sampling time ΔT. For example, from (18) and (19), the discrete value at the least time is related to the one at later time $1\Delta T$ by

$$\langle p(0\Delta T)\rangle / \langle p(1\Delta T)\rangle = 1.366. \tag{20}$$

As a practical matter, so that any direction is calculable, we replace the analytical treatment of (18)–(20) by digital integration of (17) using the DCADRE computer program integration for the Romberg technique. This method has proved to be essential close to the shadow boundary. Away from the shadow boundary the discrete pressures obtained by averaging differ from the instantaneous calculations of $p(t)$ by at most 3.5% (at $n = 1$). For simplicity, instantaneous values are used instead of average values when the discrepancy is less than 1%, i.e., for $n > 1$. This behavior is shown in Fig. 2 for a 90° wedge, where only for $n = 1$ is there a perceptible difference between the instantaneous and the average representations for $p(t)$.

Having established this digital interpretation of discrete pressures received at discrete time delays, one cannot avoid the next step in a Huygens pulse interpretation: Each received pressure was caused by a pair of weaker delta function sources (or a single source in the case of the least time path), radiating from properly positioned points on the wedge crest. We call these the "secondary sources." Their appropriate positions are calculated by the required travel times. The secondary source of $\langle p(0\Delta T)\rangle$ will be located at the point of intersection of the source–receiver axis and the crestline. It will have the fractional source strength, S_{ss} necessary for propagation from a point source,

$$S_{ss0} = F_0 S, \tag{21}$$

where

$$F_0 = \text{secondary source fraction for } 0\Delta T = \langle p(0\Delta T)\rangle / p_\delta \tag{22}$$

and

$$p_\delta = S\rho/(2\pi R\Delta T) \text{ (receiver on plane of wedge)} \tag{23}$$

or

$$p_\delta = S\rho/(4\pi R\Delta T) \text{ (receiver not on plane of wedge)}, \tag{24}$$

S = primary source strength in (1) and R = range from secondary source to receiver.

Later secondary sources come in pairs along the crest above and below the least time secondary source; each has the strength

$$S_{ssn} = F_n S, \tag{25}$$

where in the symmetrical geometry

$$F_n = (\tfrac{1}{2})\langle p(n\Delta T)\rangle / p_\delta. \tag{26}$$

The analytical theory of impulse diffraction gives no hint of the partition of pressure for asymmetrical geometries in which the $R_0' \neq R_0''$ and $R' \neq R''$ (see Fig. 4). To calculate this partition, since there is spherical divergence from the true source to the secondary source along path R_0' (or R_0'') and from secondary source to receiver along path R' (or R''), the received pressures via the two paths are

$$p'(n\Delta T) = K/(R_0'R') \text{ and } p''(n\Delta T) = K/(R_0''R''), \tag{27}$$

where K is a constant. Then, since the two components at time $n\Delta T$ are in phase, the total received pressure is

$$\begin{aligned} p(n\Delta T) &= p'(n\Delta T) + p''(n\Delta T) \\ &= K\,[(R_0'R' + R_0''R'')/(R_0'R'R_0''R'')], \quad n \neq 0. \end{aligned} \tag{28}$$

Then, after solving for K, the secondary source fractions that replace F_n in (17) for the partition of pressure in asymmetrical geometries are

$$F_n' = \frac{p'}{p_\delta} = \frac{K}{p_\delta R_0'R'} = \left(\frac{p(n\Delta T)}{p_\delta}\right)\left(\frac{R_0''R''}{R_0'R' + R_0''R''}\right) \tag{29}$$

and

$$F_n'' = \left(\frac{p(n\Delta T)}{p_\delta}\right)\left(\frac{R_0'R'}{R_0'R' + R_0''R''}\right). \tag{30}$$

II. DOUBLE DIFFRACTION: METHOD

In the discrete Huygens description of double diffraction, the objective is to find an effective digital representation of the pressure produced by the infinite number of infinitesimal sources at the first edge, each of which spawns an infinite number of diffractions at the second edge. Our simple technique starts by defining n partial least time paths from points on the first edge, past the second edge, to the receiver, such that the adjacent total paths from source to first edge to second edge to receiver differ by ΔT (Fig. 4). [The time increment ΔT is defined by the minimum bandwidth $\mathrm{BW(Min)} = (2\Delta T)^{-1}$ of the frequency response that is ultimately desired.] Each least time path defines a secondary source position on the first wedge; $\pm 1/(2\Delta T)$ defines the secondary source segment whose radiation is identified as coming from the secondary source position.

For each secondary source a virtual receiver is set up at the correct total range but on the extrapolated backside of the first wedge [Fig. 6(b)], and Eq. (1) is integrated over the time of reradiation from the secondary source segment to calculate the n pressures at ΔT increments that would have been received if there had been only a simple wedge. These

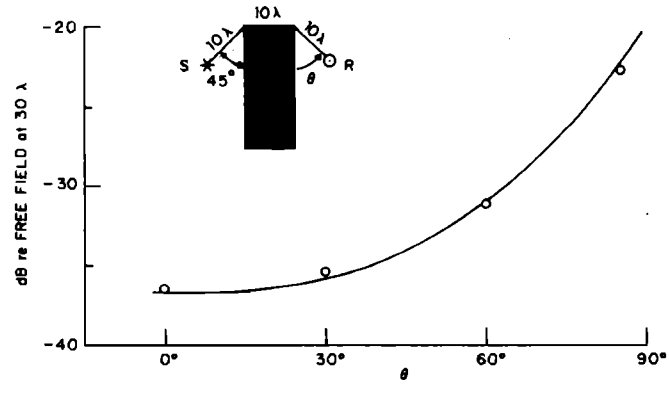

FIG. 5. Comparison of analytical solution, solid line, with discrete impulse calculations, circles, for a problem discussed by Pierce (Ref. 4).

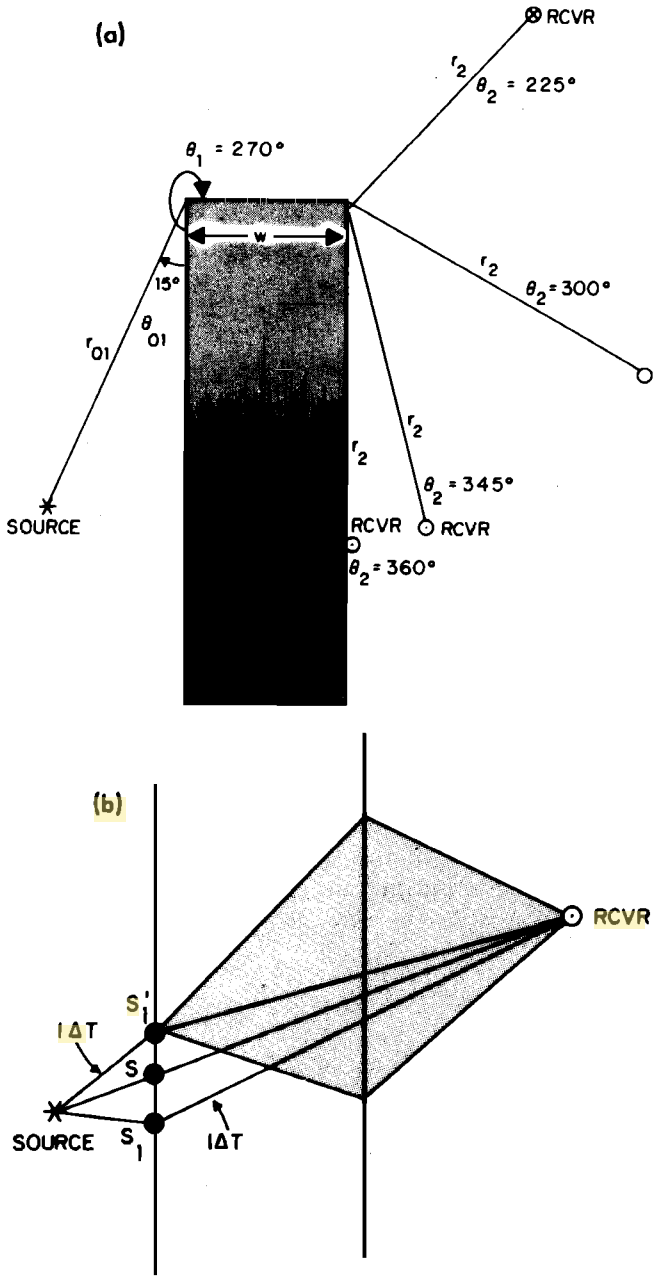

FIG. 6. (a) Double diffraction geometry for plate of thickness W. Four receiver cases are shown. For first corner $\theta_0 = \theta_{01} = 15°$; $\theta = \theta_1 = 270°$, $\theta_w = 270°$, $r_0 = r_{01} = 25$ cm, $r = W + R_2$; for second corner $\theta_0 = 0°$, $\theta = \theta_2 = 225°$, 300°, 345°, or 360°, $\theta_w = 270°$, $r_0 = W$, $r = r_2 = 25$ cm. (b) Unfolded geometry for double diffraction. Shown are the least time path from source to secondary source S to receiver, and the partial least time paths at time lag $1\Delta T$ from source to secondary sources S_1 and S_1' to receiver. Some of the reradiation from secondary source S_1' over the second wedge is indicated by shaded area.

pressures are then used in (21) and (22) and (24) to calculate the n equivalent secondary source strengths S_n. The effect of these calculations is to replace continuous line secondary source segments on the first edge by equivalent discrete delta function sources of known fractional strengths. For the finite first wedge, only a limited extent of secondary sources is possible; for a *finite* second wedge, only a finite integration of the radiation from the secondary sources is performed.

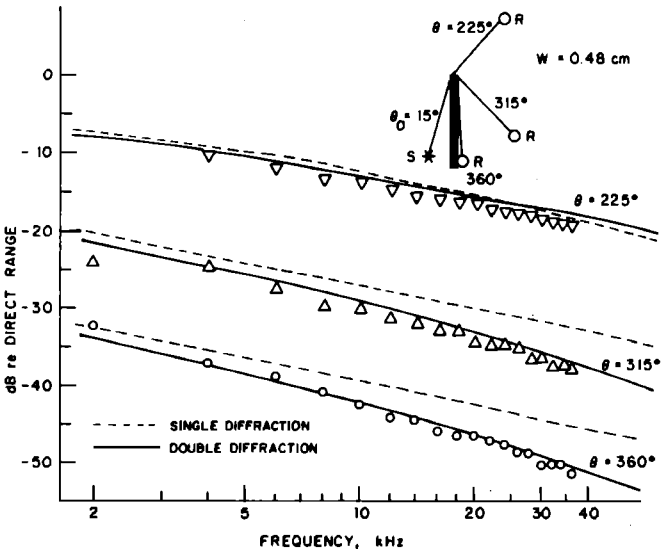

FIG. 7. Spectral loss for a thin semi-infinite plate, $\theta_w = 360°$, $W = 0.48$ cm, at incident angle 15°, received signal at 225°, 315° and 360°, $r = r_0 = 25$ cm. Dashed line is single diffraction theory [Eqs. (1)–(3)] assuming $W = 0$. Solid lines are double diffraction calculations. Experimental data from Refs. 6, 9.

The n secondary sources are used as point sources to calculate the diffracted pressures over the second wedge. The calculations are done for each secondary source using the fractional pressures to replace the unit pressures in (1). Finally, all contributions are sorted into the $n\Delta T$ cells in preparation for digital transformation to the frequency domain.

In practice, it is useful to define two criteria to make the discrete calculation both effective and efficient:

(1) The bandwidth is set at BW = 4 BW(Min). This smaller value of ΔT is used to provide more frequent sampling of the stronger early arrivals which results in more accurate integration for the discrete values.

(2) The sampling of pressures in the $p(t)$ calculation is taken to a time such that p final $\leqslant 0.05\, p(0\Delta T)$. This duration has proved to be long enough to include the major part of the diffracted energy.

The detailed effects of (1), variation of bandwidth by variation of ΔT, and (2) truncation of the discrete impulse calculation at sufficiently long times such that $p_{\text{final}} \leqslant 0.05\, p(0\Delta T)$, have been tested by the successful comparison with a cw analytical solution by Pierce[4] as shown in Fig. 5. The method has been used to compare with laboratory experiments as described in the following sections.

III. DOUBLE DIFFRACTION: COMPARISON WITH EXPERIMENT

A series of laboratory experiments was conducted to provide the spectral data to thoroughly test the impulse double diffraction method just described. All experiments were done by pulse techniques in a large anechoic chamber in order to eliminate interference from extraneous scatterers and to minimize external noise. The conventional use of a spark source was rejected as being unsuitable here because a spark source produces finite amplitude distortion which is a function of propagation range. Instead either a 2.54-cm-

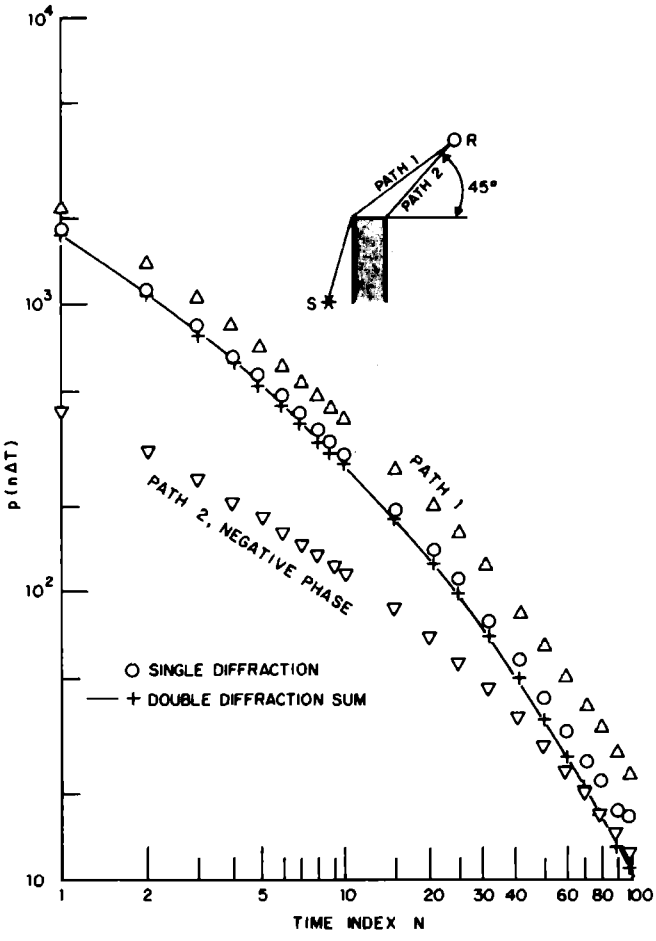

FIG. 8. Impulse solutions for plate of thickness $W = 0.48$ cm, at $\theta_0 = 15°$, $\theta = 225°$, $r = r_0 = 25$ cm. Single diffraction theory which assumes a plate of infinitesimal thickness, $W = 0$ and $\theta_w = 360°$ is designated by circles. The complete description assumes two 90° wedges at separation W, resulting in path 1, symbol Δ and path 2, symbol ∇, which is of opposite phase. Sum of paths 1 and 2 given by +.

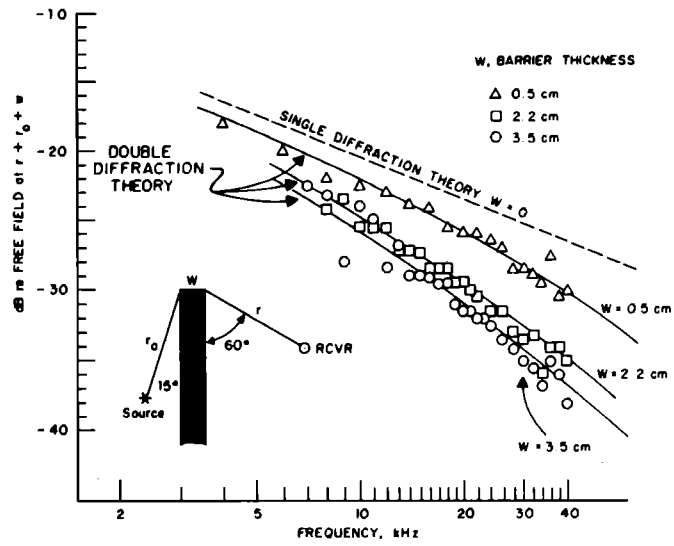

FIG. 9. Spectral loss for plates of three thicknesses at $\theta_0 = 15°$, $\theta = 300°$. Single diffraction theory, $W = 0$, $\theta_w = 360°$ is dashed line. Double diffraction calculations are solid lines with data for $W = 0.48$ cm, symbol Δ; $W = 2.2$ cm, □; and W = 3.5 cm, symbol O, from Ref. 6.

diam or a 1.27-cm-diam Bruel and Kjaer condenser microphone was polarized (at 200 V, or 250 V, respectively) and used as a source with a peak signal voltage pulse of 50 V. The spectra of the pulses were flat ± 10 dB from 2 to 16 kHz for the larger source and from 6 to 40 kHz for the smaller source.

A timing simulator (Interface Technology RS648) triggers the arbitrary waveform generator (Wavetek 175) as well as the time-lagged 12-bit A/D converter and computer sampling frequency oscillator. The signal is typically sampled at 320 000 s^{-1} in a block of 128 points (0.4 ms) for a resolution of 2.5 kHz. A new block is triggered approximately every 80 ms and coherent averaging of either 1000 or 10 000 blocks is performed before the fast-Fourier transform is applied. Details of the system are in Refs. 6 and 9.

IV. PLATES

Our previous experimental studies of shadowing by a semi-infinite plane (thin plate), in fact used a plate that was 0.48 cm thick. Although the agreement between single diffraction thin plate theory [Eq. (1)] and experiment was excellent (less than 1 dB discrepancy) when $\theta \leqslant 270°$, much larger discrepancies were observed[5,9] when the angles were larger than 270°. It is now possible to predict the experimental results by using the discrete double diffraction calculation. The method is to interpret the geometry as two contiguous 90° wedges separated by the plate thickness W, as shown in Fig. 6.

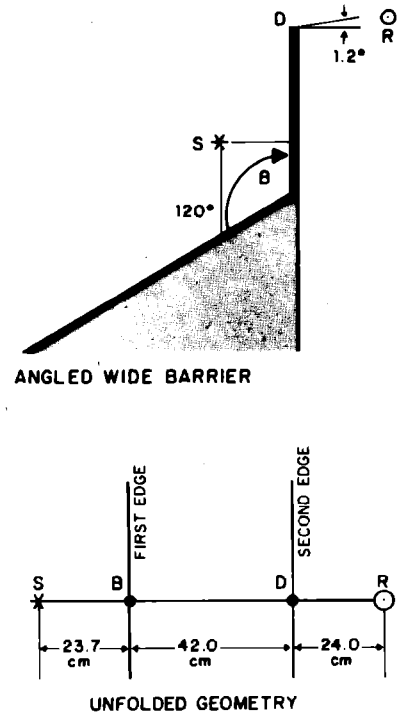

FIG. 10. Geometry of the angled wide barrier above, and unfolded, below. For the wedge at B, the parameters are $\theta_0 = 64.7°$, $\theta = 120°$, $\theta_w = 120°$, $r_0 = 23.7$ cm, $r = 42.5$ cm. For the second wedge at D, $\theta_0 = 0°$, $\theta = 268.8°$, $\theta_w = 360°$, $r_0 = 42.5$ cm, $r = 24.0$ cm.

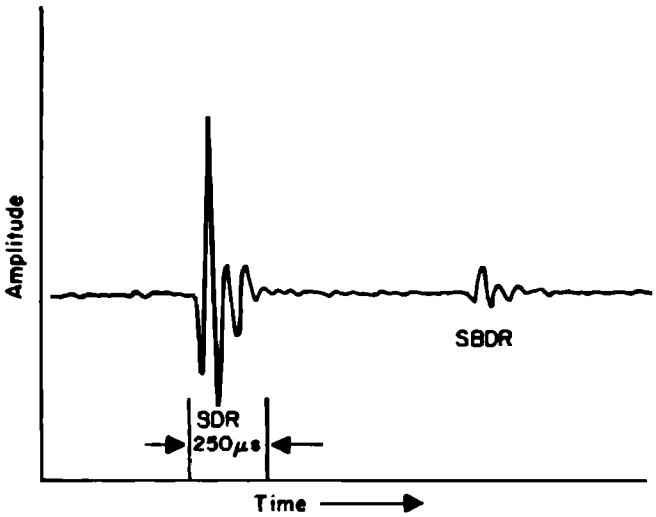

FIG. 11. Oscilloscope pattern of signal via the single diffraction path SDR followed by the double diffraction via SBDR (see Fig. 10). The relative amplitudes in this figure are affected by the beam pattern of the source.

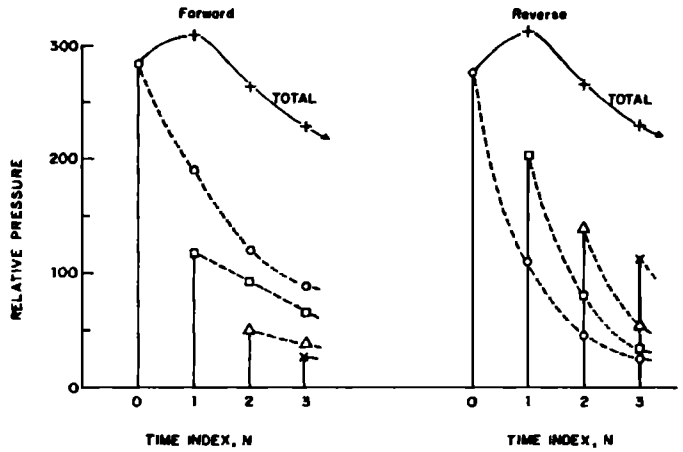

FIG. 13. Discrete pressures diffracted by an angled wide barrier forward, path SBDR, and reversed, path RDBS. See Figs. 10–12. Four least time contributions shown for each case; dashed lines join the secondary diffractions that follow them.

Figure 7 presents the spectral predictions and experimental data for three receiver angles for plate thickness $W = 0.48$ cm. At $\theta = 225°$, the thin plate theory appears to work well enough; discrete double diffraction theory is almost inseparable from the single diffraction thin plate theory. At $\theta = 315°$ and $\theta = 360°$, however, thin plate theory is off by significant amounts: rms discrepancies are 3.9 and 4.0 dB, respectively. Discrete double diffraction calculations show a much improved agreement with experiment: rms discrepancies are only 1.1 and 0.7 dB, for $\theta = 315°$ and 360°.

The explanation of the spectral results at $\theta < 270°$ is found in the time domain, Fig. 8. The impulse response for the "naive" application of thin plate theory for $\theta = 225°$ is almost identical to the sum of the single diffraction from the first corner plus the double diffraction *of opposite phase* from the second corner. When the plate is thicker and $\theta < 270°$, the importance of the double diffraction path becomes even greater, for now the negative phase component is delayed significantly because of the longer path for double diffraction *re* single diffraction.

For receiving angles greater than 270°, however, there is no single diffraction path, and the double diffraction interpretation is essential. Consider the case $\theta = 300°$ for three different plate thicknesses, Fig. 9. Thin plate theory is in error by 2.7 dB (rms discrepancy) for the plate $W = 0.48$ cm, and of order 5 to 10 dB for the thicker plates; discrete double diffraction shows rms discrepancies of only 0.6, 0.6, and 1.0 dB for the plates of widths 0.48, 2.2, and 3.5 cm, respectively.

V. ANGLED WIDE BARRIER

Consider the wide double barrier made up of a ramp of slope 60° with the vertical, topped by a vertical barrier, Fig.

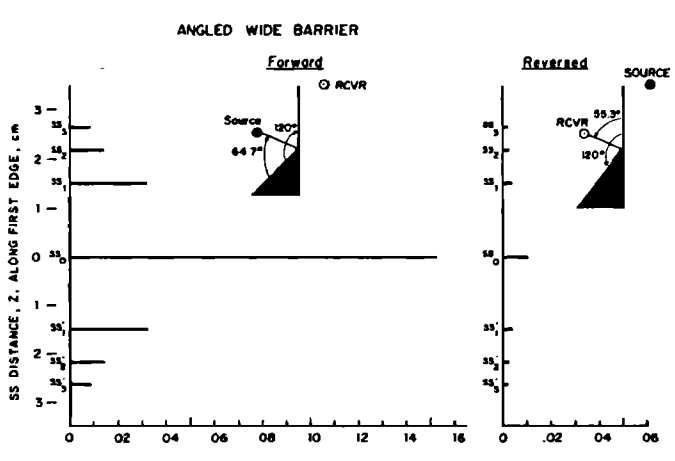

FIG. 12. Seven secondary source fractions for each of two experiments: angled wide barrier, forward and reversed. The primary source strength is unity; e.g., SS_0 for the forward case represents a secondary source 15.2% as great as the primary delta function source.

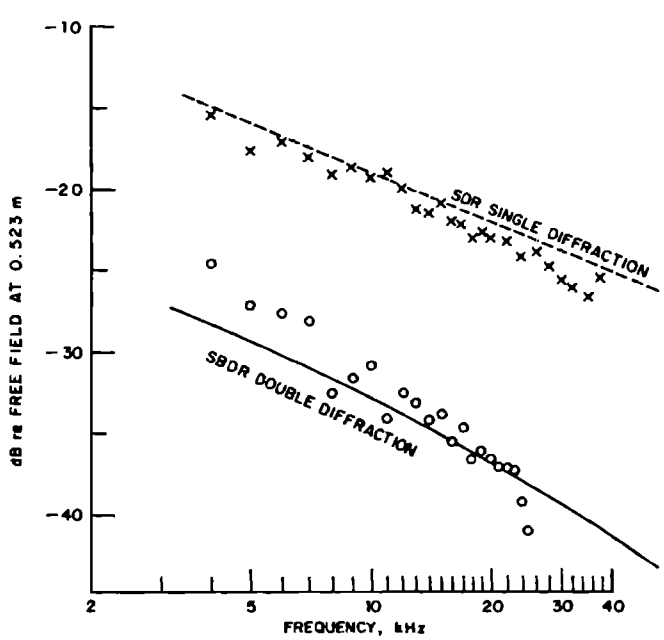

FIG. 14. Spectral loss *re*: free-field divergence for angled wide barrier, Fourier transformed from curves of Fig. 13.

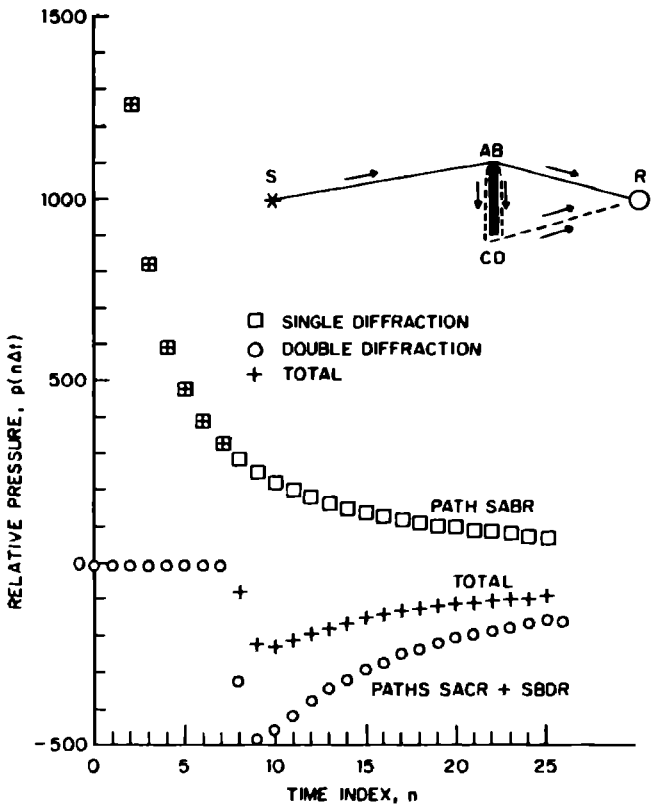

FIG. 15. Strip diffraction. For the upper paths the total pressure-time behavior is the sum of the single diffraction contribution by path SABR and those by double diffraction paths SACR and SBDR. The symmetrical lower paths such as SCDR are not shown here.

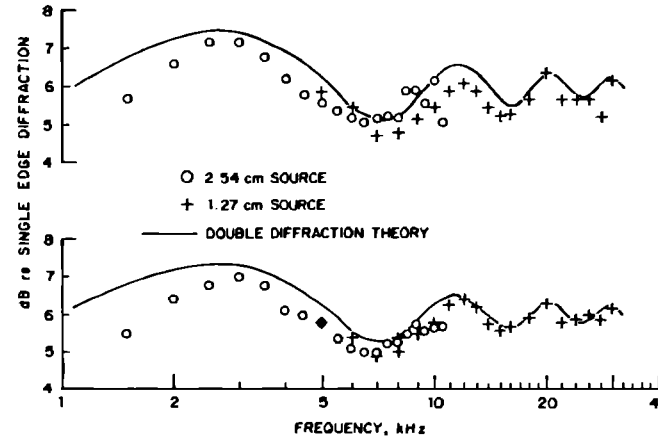

FIG. 16. Spectra of diffracted pressure of a 4-cm strip relative to that of a single edge. Data circles were obtained with a 2.54-cm-diam source, crosses with a 1.27-cm-diam source. Double diffraction theory is the solid line, with plates assumed to have zero thickness. Source to strip, 14.5 cm. Strip to receiver, 9.5 cm upper graph, 23.2 cm lower graph.

10. In this case two signals are seen, Fig. 11, the first caused by single diffraction over the vertical barrier (path SDR), the second by double diffraction. The double diffraction path scatters first from the 120° angle between the incline, then over the vertical barrier (path SBDR).

We assume that the vertical barrier is a thin plane ($\theta_\omega = 360°$) for this digital solution, and we are concerned principally with the double diffraction path SBDR. The easily calculated contributions due to mirror images in the base have been discussed previously[5] and will not be repeated here.

For interest, and to check reciprocity, the calculation has been done for the source–receiver positions of the laboratory experiment and also for the reversed positions. The secondary source strengths and their positions on the first edges of the two cases are presented in Fig. 12. For the forward configuration the axial strength SS_0, located on the line at the apex of the 120° angle, is dominant. For the reversed condition, when the secondary source line is on the edge of the vertical barrier, there is a more nearly even distribution of secondary source strengths. Nevertheless, when the secondary reradiation is considered, Fig. 13, the slower rate of decay of the radiation from SS_1, SS_2, SS_3, etc. in the forward case, results in the *sum* of the doubly diffracted pressures being essentially the same, forward or reversed. Reciprocity is thereby confirmed.

The transform into the frequency domain is presented in Fig. 14. The rms discrepancy for the double diffraction path SBDR, when compared with experiment, is 1.5 dB.

VI. STRIP

Our final example is the case of diffraction by a strip. This is a classical problem which is commonly described by use of the Helmholtz–Kirchhoff integral.[10] However, the Kirchhoff assumption, which is generally used in these solutions, is not valid except in directions close to the normal to the strip.[7,8] In fact, the component of scatter along the plane of the strip is a significant factor in the total solution, as the following experiments show.

The geometry of the strip experiment and the pressure-time behavior is sketched in Fig. 15. The sound follows three principal paths (and their symmetrical counterparts not shown): the single diffraction trajectory SABR; and the double diffraction paths SACR along the front face AC and SBDR along the shadowed face BD. The latter two paths indeed show the same amplitudes but opposite phase shifts at AB and then reversed phase shifts at CD so that the pulse that propagates from CD to R is a *double* pulse which arrives at a delayed time relative to the single diffraction path SABR. The event occurs at approximately $n = 8$, where $T = 7.8$ ms in this case.

If the double diffraction path did not exist the situation could be represented by the sum of the single diffractions from two semi-infinite planes; the diffraction field for the strip would be 6 dB greater than the field from a single infinite plate. The double diffraction paths strongly perturb this simple addition with a periodicity that depends on the strip width. The theoretical and experimental spectra are presented in Fig. 16 for a 4-cm-wide strip, viewed from two ranges. The periodicity of the interference effect is about 8 kHz, approximately $(2n\Delta T)^{-1}$ as expected. The curve of the double diffraction theory is essentially correct; the rms discrepancy is approximately 0.5 dB.

VII. CONCLUSION

The discrete Huygens impulse calculation provides accurate solutions to problems involving double diffraction.

ACKNOWLEDGMENT

This research was supported by the Office of Naval Research.

[1]J. J. Bowman, T. B. A. Senior, and P. L. E. Uslenghi, *Electromagnetic and Acoustic Scattering by Simple Shapes* (North-Holland, Amsterdam, 1969).

[2]H. G. Garnir, Bull. Soc. Roy. Sci. Liege **3**, 119 (1952); **3**, 207 (1952); **3**, 328 (1952).

[3]M. A. Biot and I. Tolstoy, "Formulation of wave propagation in infinite media by normal coordinates with an application to diffraction," J. Acoust. Soc. Am. **29**, 381–391 (1957). See also I. Tolstoy, *Wave Propagation* (McGraw-Hill, New York, 1973).

[4]A. D. Pierce, *Acoustics* (McGraw-Hill, New York, 1981), pp. 489–490; see also J. Acoust. Soc. Am. **55**, 941–955 (1974).

[5]H. Medwin, "Shadowing by finite barriers," J. Acoust. Soc. Am. **69**, 1060–1064 (1981).

[6]G. M. Jebsen, "Acoustic diffraction by a finite barrier: Theories and experiment," M. S. thesis, Naval Postgraduate School, Monterey, CA 93940 (March 1981).

[7]W. A. Kinney, C. S. Clay, and G. A. Sandness, "Scattering from a corrugated surface: comparison between experiment, Helmholtz–Kirchhoff theory and the wedge-ensemble method," J. Acoust. Soc. Am. **72** (1982) (in press).

[8]G. M. Jebsen and H. Medwin, "On the failure of the Kirchhoff Assumption in backscatter," J. Acoust. Soc. Am. **72** (1982) (in press).

[9]J. H. Bremhorst "Impulse wave diffraction by rigid wedges and plates," M. S. thesis, Naval Postgraduate School, Monterey, CA 93940 (December 1978).

[10]M. Born and E. Wolf, *Principles of Optics* (Pergamon, New York, 1970), Chap. 8, pp. 448–452.